Pergamon

Cement and Concrete Research, Vol. 27, No. 3, pp. 437-451, 1997

0008-8846/97 $17.00 + .00

PII S0008-8846(97)00013-6

# EVALUATION OF THE INTERFACIAL SHEAR IN A DISCONTINUOUS CARBON FIBER/MORTAR MATRIX COMPOSITE

**Mingguang Zhu, Robert C. Wetherhold and D.D.L. Chung**
Composite Materials Research Laboratory
State University of New York at Buffalo, Buffalo, NY 14260-4400

(Refereed)
(Received June 25, 1996; in final form January 21, 1997)

## ABSTRACT

The mathematical relationship between fiber-matrix interfacial shear stress and drying shrinkage reduction due to fiber addition was derived for the purpose of estimating this stress from the measured drying shrinkage of short fiber reinforced cement. For short carbon fiber reinforced mortar, this stress increased with curing age, particularly abruptly within the first 2 days and reaching 1.92 MPa at 14 days if slip between fiber and matrix was assumed and 3.46 MPa if no slip between fiber and matrix was assumed. © *1997 Elsevier Science Ltd*

## Introduction

Concrete reinforced with short fibers (e.g., steel, carbon, polymer) is attractive due to its high flexural toughness and low drying shrinkage, and, in some cases, high tensile and flexural strength [1-7]. The bond between fiber and cement matrix is critical to the effectiveness of the fibers, particularly in relation to drying shrinkage and strength. The ability of the fibers to decrease the drying shrinkage largely depends on the fiber-matrix interfacial shear stress. Although a close relationship between this stress and the drying shrinkage is intuitively clear, no mathematical relationship between these quantities has been previously reported. This relationship allows estimation of the interfacial shear stress from measured drying shrinkage data. Although the interfacial shear strength can be measured by single fiber pull-out testing [8-14] and indentation testing [15], these tests are tedious and destructive. In contrast, measurement of the drying shrinkage is simple and non-destructive. The objective of this paper is the development of the relationship between drying shrinkage and interfacial shear stress.

Although the relationship between the interfacial shear stress and the drying shrinkage has not been previously reported, that between this stress and the tensile stress/strain has. In a study of a copper-matrix/aligned tungsten fiber composite, by assuming that the interfacial stress is a constant and modeling the matrix as a rigid, perfectly plastic material, Kelly and Tyson [16] derived the relationship between tensile strengths of matrix and composite and the interfacial stress:

$$\sigma_c = V_f \frac{\tau_e L}{r} + V_m \sigma_m$$

$$\tau_e = \frac{\sigma_c - V_m \sigma_m}{s V_f}$$

where $\tau_e$ = interfacial shear stress = matrix yield stress in shear, $L$ = half of fiber length, $r$ = half of fiber diameter, $s$ = L/r = aspect ratio of fiber, $V_m$ = volume fraction of matrix, $V_f$ = volume fraction of fiber, $\sigma_m$ = tensile strength of matrix, and $\sigma_c$ = tensile strength of composite. In studying the interfacial bonding behavior of composites under tensile stress, Cox and Piggott [17-19] derived the interfacial shear strength $\tau_e$ as a function of tensile strain of matrix ($\epsilon_m$) and composite ($\epsilon_c$), elastic modulus of fiber ($E_f$), aspect ratio of fiber ($s$) and distance from center to end of fiber (x), i.e., $\tau_e = F(\epsilon_m, \epsilon_c, E_f, s, x...)$ (by assuming that there is no slip between fiber and matrix). In this paper, we formulate a relationship similar to the formulae in [16-19] for the case in which the fibers possess angular orientation in three dimensions.

Carbon fibers were chosen for this study, due to the low drying shrinkage, high tensile and flexural strength [5,20-27] and strain sensing ability [28-33] of cement with short carbon fibers.

## Theory

Cementitious materials shrink during curing and hardening because of the hydration reaction and the withdrawal of water. Obviously, if the mortar shrinkage occurs during its plastic stage

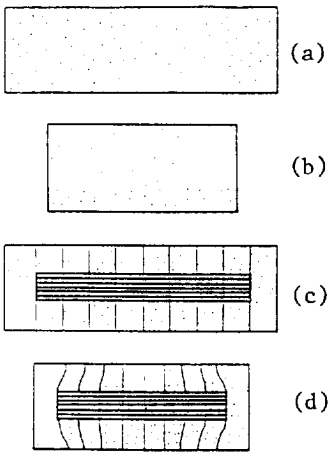


FIG. 1.
Mortar shrinkage elements. (a) Plain mortar before shrinkage. (b) Plain mortar after shrinkage. (c) Composite mortar before shrinkage. (d) Composite mortar after shrinkage.

(which is called the plastic shrinkage), there will be no stress at the fiber/mortar interface. However, if the mortar shrinks at its hardening stage (which is called drying shrinkage), interfacial stress between fiber and mortar matrix will be generated. Fig. 1 shows that the drying shrinkage of a fibrous composite mortar is smaller than that of plain mortar. This means that a certain amount of internal or self-equilibrating force (i.e., fiber-matrix interfacial force) restricts the shrinkage of the matrix. Therefore, by investigating the stress-strain behavior and using the principle of force equilibrium, it is possible to find the relationship between drying shrinkage and the fiber-matrix interfacial shear stress. In this paper, two mathematical models which predict the shear stress between fiber and matrix through the shrinkage strain were derived. They are called the Slip Model and the No Slip Model. Both models use the following simplifying assumptions. (1) The matrix and the fiber are both elastic materials. (2) The interface is infinitesimally thin. (3) The properties of the matrix in the vicinity of the fiber are the same as those of the bulk matrix. (4) No stress is transmitted through the fiber ends. (5) There is no effect of the stress field around one fiber on neighboring fibers. Assumption (5) is reasonable since the fiber content is normally < 2 vol.%.

Slip Model. This model assumes that there exists a constant interfacial shear stress $\tau_c$ along the entire fiber-matrix interface (Fig. 2). This assumption is appropriate if the bond strength is negligible, there is frictional sliding at the fiber-matrix interface (shown by pull-out testing [34]), and the Poisson effect on the fiber is small enough that the interface pressure can be assumed constant. The stress-strain behavior of a mortar is non-linear. However, since the drying shrinkage is small, we may treat the mortar as a linear elastic material during the shrinkage.

Consider a plain mortar and a composite unit and their associated shrinkage during curing (Fig. 1). For plain mortar, the stress-strain relationship in the longitudinal direction is

$$\epsilon_m = \frac{\sigma}{E_m} + \epsilon_m^s ,$$

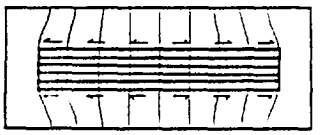

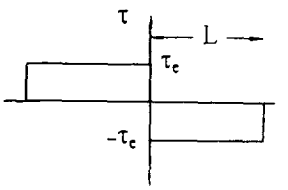


FIG. 2.
Singe fiber composite element. (a) Stressed single fiber composite element. (b) Fiber-matrix interfacial stress which causes less shrinkage of composite mortar than plain mortar.

where $\epsilon_m$ = overall strain of plain mortar, $\sigma$ = stress applied on mortar parallel to the longitudinal direction, $E_m$ = elastic modulus of mortar, and $\epsilon_m^s$ = shrinkage strain of mortar during curing in the longitudinal direction. By considering free shrinkage of the mortar, i.e., assuming $\sigma = 0$, we have

$$\epsilon_m = \epsilon_m^s ,$$

where $\epsilon_m^s$ as a function of time can be obtained through experiments.

For the mortar matrix in the composite, there exists an internal stress which results from the fiber-matrix interfacial restricting force. Thus, the axial direction stress-strain relationship of the mortar matrix in the composite during curing is

$$\epsilon_{m\text{-}c}^s = \frac{\sigma_i}{E_m} + \epsilon_m^s , \tag{1}$$

where $\epsilon_{m\text{-}c}^s$ is the overall strain of the mortar matrix in the composite, and $\sigma_i$ is the internal stress applied on the mortar matrix which results from the fiber-matrix interfacial restricting force. This restricting force causes the composite mortar to have less drying shrinkage than the plain mortar. By assuming that carbon fibers do not change dimensions during the curing of the mortar, we can consider that the overall strain of the mortar matrix is equal to the drying shrinkage of the whole composite, i.e.,

$$\epsilon_{m\text{-}c} = -\epsilon_c^s ,$$

where $\epsilon_c^s$ is the drying shrinkage strain of the whole composite. Thus, from this assumption and Eq. (1),

$$\sigma_i = E_m(\epsilon_{m\text{-}c}^s - \epsilon_m^s) \tag{2a}$$

The shrinkage strain of mortar matrix $\epsilon_{m\text{-}c}^s$ varies along the length of fiber, i.e.,

$$\epsilon_{m\text{-}c}^s = \epsilon_{m\text{-}c}^s (x)$$

The distribution of the shrinkage strain is complex. However, the average value of the drying shrinkage of mortar matrix can be obtained through measurement. Thus, by using the average value of the shrinkage strain $\bar{\epsilon}_{m\text{-}c}^s$ (instead of $\epsilon_{m\text{-}c}^s(x)$), Eq. (2a) can be rewritten as

$$\bar{\sigma}_i = E_m (\bar{\epsilon}_{m\text{-}c}^s - \epsilon_m^s) , \tag{2b}$$

where $\bar{\sigma}_i$ is the average internal stress applied on the mortar matrix by the fiber-matrix interfacial stress. Using the symbol $\epsilon_1$ for the composite mortar shrinkage $\bar{\epsilon}_{m\text{-}c}^s$ minus the plain mortar drying shrinkage $e_m^s$, i.e., $\epsilon_1 = \bar{\epsilon}_{m\text{-}c}^s - \epsilon_m^s$, Eq. (2b) can be written as

$$\bar{\sigma}_i = E_m \epsilon_1 \tag{3}$$

Eq. (3) means that the internal stress applied on the mortar matrix, as caused by the fiber-

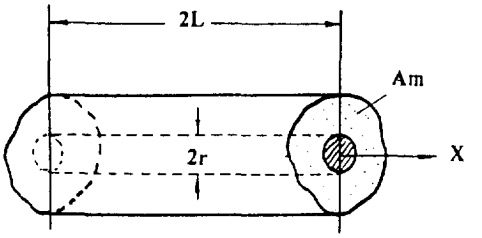


FIG. 3.
Single fiber composite element.

matrix interfacial force, is equal to the elastic modulus of the matrix times the drying shrinkage difference between plain mortar and composite mortar. In other words, the fiber-matrix interfacial force generates an internal stress on the mortar matrix. This internal stress "pulls" the composite mortar by strain $\epsilon_1$, which equals the average composite mortar shrinkage $\bar{\epsilon}^s_{m\text{-}c}$ minus the plain mortar drying shrinkage $\epsilon^s_m$.

Fig. 3 shows a composite mortar unit - a fiber of length *2L* surrounded by the matrix. By assuming that the interface has constant shear stress $\tau_e$ and considering equilibrium,

$$\tau_e 2\pi r \cdot 2L = \bar{\sigma}_i \cdot A_m \ , \tag{4}$$

where $A_m$ is the cross-sectional area of the matrix. Thus, the volume fraction of fibers $V_f$ is

$$V_f = \frac{\pi r^2}{A_m} \tag{5}$$

Introducing Eq. (3) and (5) into (4) and simplifying,

$$\tau_e = \frac{E_m}{4sV_f} \epsilon_1 \ , \tag{6}$$

where s is the aspect ratio of carbon fibers ($s = L/r$). Thus, by measuring the drying shrinkage of both plain mortar and composite mortar, the interfacial shear stress can be calculated.

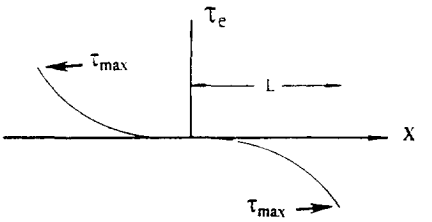


FIG. 4.
Fiber-matrix interfacial stress.

No Slip Model. In the No Slip Model, it is assumed that both fibers and matrix behave elastically, and that the interface transfers the stress from fibers to matrix without yielding or slip. Following [19], the drying shrinkage difference $\epsilon_1$ and the interfacial shear stress $\tau_e$ are related:

$$\tau_e = \frac{1}{2} n E_f \epsilon_1 \frac{\sinh(nx/r)}{\cosh(ns)} \tag{7}$$

As shown in Fig. 4, when $x=L$, $\tau_e = \tau_{e_{max}}$. Thus we have

$$\tau_{e_{max}} = \frac{1}{2} n E_f \epsilon_1 \tanh(ns) \ , \tag{8}$$

where

$$n = \left( \frac{2E_m}{E_f(1+\nu_m)\ln(P_f/V_f)} \right)^{1/2} \tag{9}$$

and $P_f$ is the packing factor which will be discussed later in this paper.

Calculation of Fiber-Matrix Interfacial Shear Stress from the Measured Drying Shrinkage. In order to calculate the shear strength between carbon fiber and cement matrix by using Eq. (6) and (8), the following parameters must be determined:

(1) s, the aspect ratio of the carbon fiber. The average fiber length (2L) and average fiber diameter (d) are used, i.e., s = 2L/d = 5 mm/10 μm = 500.

(2) $\nu_m$, the Poisson's ratio of the mortar. The values of the Poisson's ratio can be obtained by direct measurement [35] or dynamic determination [36,37]. The reported value of the Poisson's ratio varies from 0.11 to 0.24 for concrete [35-37]. No reported value of the Poisson's ratio of plain mortar was found. Also, there is no reliable information on the variation in the Poisson's ratio with age, strength, or other properties of concrete. However, it is generally believed that the Poisson's ratio is lower in high strength

TABLE 1

Properties of Carbon Fibers. (From data sheet of Ashland Petroleum Co.)

| | |
|---|---|
| Nominal length | 5 mm |
| Filament diameter | 10 μm |
| Tensile strength | 690 MPa |
| Tensile modulus | 48 GPa |
| Elongation at break | 1.4% |
| Electrical resistivity | $3.0 \times 10^{-3}$ Ω.cm |
| Specific gravity | 1.6 g $cm^{-3}$ |
| Carbon content | 98 wt.% |

TABLE 2

Compressive modulus of Plain Mortar at Different Curing Ages

| Curing age (days) | Compressive modulus (GPa) |
|---|---|
| 0.3 | 2.74 ± 9.5% |
| 0.5 | 3.75 ± 5.7% |
| 0.75 | 4.18 ± 4.3% |
| 1.0 | 4.83 ± 4.2% |
| 2.0 | 5.57 ± 7.4% |
| 4.0 | 6.37 ± 6.9% |
| 6.0 | 6.41 ± 12.2% |
| 8.0 | 6.73 ±3.9% |
| 10.0 | 6.79 ± 10.7% |
| 12.0 | 6.85 ± 9.1% |
| 14.0 | 7.01 ± 5.8% |

concrete [38]. Here, we treat the Poisson's ratio as a constant with a value of $v_m = 0.2$. (In the later calculation, it was found that the change of Poisson's ratio by 10% would only change the calculated interfacial shear stress by 0.8%).

(3) $E_f$, the elastic modulus of the carbon fiber. From Table 1, $E_f = 48$ GPa.

(4) $V_f$, the fiber volume fraction in the composite mortar. In practice, 0.35 vol.% of carbon fibers provided mortar that gave the highest brick-mortar bond strength [39].

(5) $E_m$, the elastic modulus of plain mortar. Similar to the variation of the mortar strength with the curing age, $E_m$ varies with the curing age. Table 2 shows the measured compressive elastic modulus of plain mortar at different curing ages. The composition and preparation of the mortar are as described in [39]. The specimen size for measuring the compressive modulus was 50.8 × 50.8 × 50.8 mm (2 × 2 × 2 in), according to ASTM Standard 109-80. Six samples were measured for each data. The load applied was 400 N. A cementitious material is not a truly elastic material [40]. It deforms at a load partly as a result of elastic strain, and partly as a result of plastic strain or creep. The compressive stress-strain curves of plain mortar after 14 days of curing in Fig. 5(a) and (b) also demonstrate that the stress-strain relationship for plain mortar is not linear, or the elastic modulus varies at different stress or strain points. In practice, one uses the average modulus [41] to refer to the elastic modulus of a cementitious material. From Fig. 5, when the maximum compressive stress is 9.6 MPa, the average modulus is 7.0 GPa (Fig. 5(a)). However, when the maximum pressure is increased to 120 MPa, the average modulus is increased to 25 GPa (Fig. 5(b)). Since the stress generated by the drying shrinkage is small, the maximum load of 400 N or the maximum pressure of 9.6 MPa is used to obtain the mean elastic modulus of 7.0 GPa.

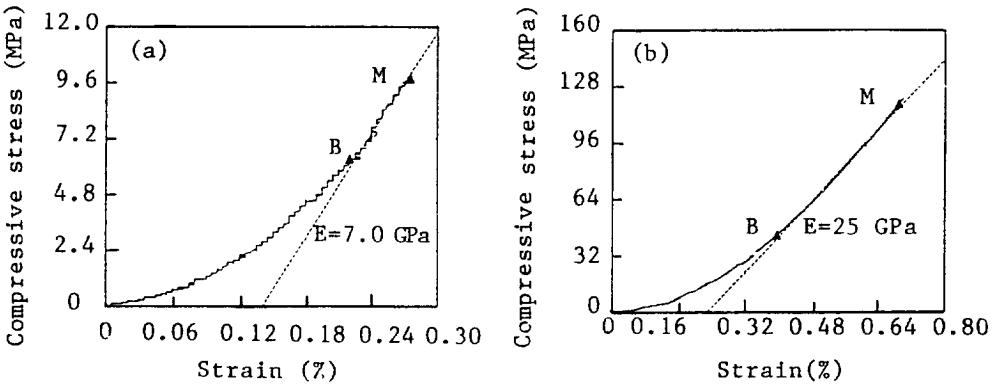


FIG. 5.

(a) Stress-strain curve of mortar block under small load. B: the beginning point to measure the modulus; M: the end point to measure the modulus. Dashed line: the mean slope of the stress-strain curve or the average elastic modulus from B to M. (b) Stress-strain curve of mortar block under large load. B: the beginning point to measure the modulus; M: the end point to measure the modulus. Dashed line: the mean slope of the stress-strain curve or the average elastic modulus from B to M. It is believed that the concave part at the beginning of the curve is mainly non-parallel seating related. The non-linearity between B and M of the curve is mainly due to the non-linear stress-strain behavior of the mortar.

(6) $P_f$, the packing factor. Usually two regular packing patterns, namely square packing and hexagonal packing, are considered. As derived by Piggott [19], $P_f = \pi$ for square packing and $P_f = 2\pi/\sqrt{3}$ for hexagonal packing. Here, we assume that $P_f$ is the average of the values for square packing and hexagonal packing, i.e., $P_f = 3.38$.

(7) $K$, the porosity factor. When carbon fibers are added to the mortar, the porosity of the mortar increases [39]. The decreased drying shrinkage is not only due to the fiber-matrix interface, but also the pores. For 0.35 vol.% carbon fiber reinforced mortar, it is assumed that K = 0.5. In other words, we assume that 50% of drying shrinkage difference was contributed by the increased porosity.

(8) $\epsilon_l$, the drying shrinkage in the fiber axis direction. In deriving the models, only shrinkage in the fiber axis direction was considered. However, in reality, the effect on mortar drying

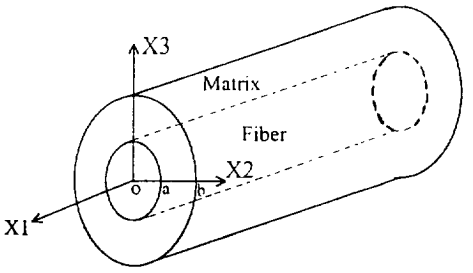


FIG. 6.

Representative volume element for aligned discontinuous fiber composite.

shrinkage in the transverse direction and the fact that fibers are three-dimensionally oriented must be counted.

First, consider a representative volume element (RVE) consisting of a short fiber embedded in a cylinder of mortar matrix (Fig. 6). The shrinkage strains $\epsilon_2$ and $\epsilon_3$ in $X_2$ or $X_3$ directions respectively must be found. We assume that the effect of the shear strain is negligible, i.e., $\epsilon_{12} = \epsilon_{13} = \epsilon_{23} = 0$ for RVE. Also, since the RVE is an axisymmetrically loaded member, we have

$$\epsilon_2 = \epsilon_3 = \epsilon_r$$

For axisymmetrically loaded members, under the condition of plain strain and the assumption that the matrix shrinkage is uniform throughout the RVE cross-section ($\epsilon_m$ = constant) [42],

$$u = \frac{(1+\nu)\epsilon_m}{(1-\nu)r}\int_a^r r dr + C_1 r + \frac{C_2}{r} \tag{10}$$

$$\sigma_r = \frac{E\epsilon_m}{1+\nu}\left[-\frac{(1+\nu)}{(1-\nu)r^2}\int_a^r r dr + \frac{C_1}{1-2\nu} - \frac{C_2}{r}\right] \tag{11}$$

where $\epsilon_m$ is the drying shrinkage strain of mortar matrix, and u is the displacement in the r direction and $\sigma_r$ is the stress in the radius direction. Under the boundary condition of $u|_{r=b} = 0$ and $u|_{r=a} = 0$ (i.e., assuming no fiber radius dimensional change), $C_1$ and $C_2$ can be found. By definition,

$$\epsilon_r|_{r=b} = \frac{u(b)}{b} \tag{12}$$

Substituting $C_1$ and $C_2$ into Eq. (10) and from Eq. (12), we have

$$\epsilon_r|_{r=b} = 74.63\times10^{-3}\epsilon_m + 144.75\times10^{-6} \tag{13}$$

The solutions found for radial and axial strains of an RVE are in the coordinate system of that RVE. In an actual sample, fibers are oriented in various directions. We must therefore transform the RVE strains into a global coordinate system, and perform orientation averaging over all of the RVE orientations. Consider an off-axis fiber (Fig. 7). The shrinkage in the fiber axis direction is

$$\epsilon_c = \epsilon_1 l^2 + \epsilon_2 m^2 + \epsilon_3 n^2 ,$$

where $l = \cos(e_f e_{x1})$, $m = \cos(e_f e_{x2})$, and $n = \cos(e_f e_{x3})$. Since $\epsilon_2 = \epsilon_3 = \epsilon_r$,

$$\epsilon_c = \epsilon_1 l^2 + \epsilon_r(m^2+n^2) \tag{14a}$$

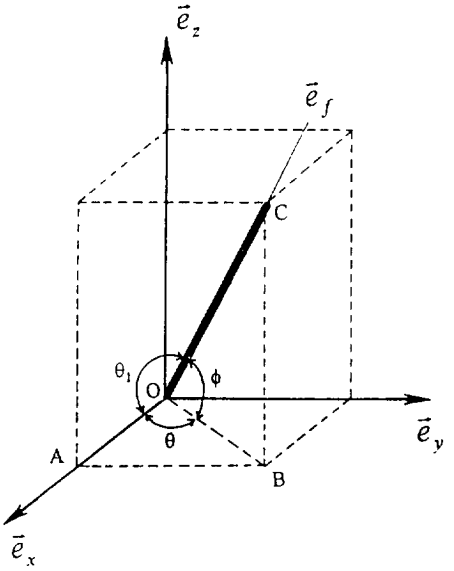


FIG. 7.
Fiber orientation angles.

As shown in Fig. 7, we can also use in-plane ($\theta$) and out-of-plane ($\phi$) angles to describe the fiber orientation. From the trigonometric relation between $\Delta ACO$ and $\Delta ACB$ (which can be represented by the fiber length OC, $\theta_1$, $\theta$ and $\phi$; also note that the two triangles shear along the same edge AC), and consider the fact that $l^2 + m^2 + n^2 = 1$, it can be found that

$$l^2 = \cos^2\phi \cos^2\theta$$

$$m^2 + n^2 = 1 - \cos^2\phi \cos^2\theta$$

Thus, Eq. (14a) becomes

$$\epsilon_c = \epsilon_1 \cos^2\phi \cos^2\theta + \epsilon_r(1 - \cos^2\phi \cos^2\theta) \tag{14b}$$

For random three-dimensionally oriented short fibers, we must find the average value

$$\langle \epsilon_c \rangle = \epsilon_1 \langle l^2 \rangle + \epsilon_2 \langle m^2 + n^2 \rangle$$

$$\langle \epsilon_c \rangle = \epsilon_1 \langle \cos^2\phi \cos^2\theta \rangle + \epsilon_2 \langle 1 - \cos^2\phi \cos^2\theta \rangle \tag{14c}$$

The probability that a fiber has orientation at in-plane angle $\theta$ and out-of-plane angle $\phi$ is defined as the distribution function

$$\langle f(\theta,\phi)\rangle = \int_{-\frac{\pi}{2}}^{\frac{\pi}{2}} \int_{-\frac{\pi}{2}}^{\frac{\pi}{2}} f(\theta,\phi) n_{\theta\phi} \cos\phi \, d\theta \, d\phi \tag{15}$$

Jain and Wetherhold [43] summarized the density function $n_{\theta\phi}\cos\phi$ under different fiber orientation conditions. For the case of uniform distribution on a unit sphere, it is

$$n_{\theta\phi}\cos\phi = \frac{1}{2}\pi \cos\phi$$

Thus, from Eq. (14c), (16) and (17), we have

$$\langle \cos^2\phi \cos^2\theta \rangle = \frac{\pi}{2} \int_{-\frac{\pi}{2}}^{\frac{\pi}{2}} \int_{-\frac{\pi}{2}}^{\frac{\pi}{2}} \cos^3\phi \cos^2\theta \, d\theta \, d\phi = \frac{\pi^2}{4} \tag{16}$$

TABLE 3

Drying Shrinkage* for Plain Mortar and 0.35 vol.% Carbon Fiber Reinforced Mortar at Different Curing Ages (From [39])

| Curing age (days) | Drying shrinkage strain ($10^{-3}$) | |
|---|---|---|
| | 0% C-fiber ($\varepsilon_m$) | 0.35 vol.% C-fiber ($\varepsilon_c$) |
| 0.3 | 1.393 | 0.689 |
| 0.5 | 1.403 | 0.717 |
| 0.75 | 1.433 | 0.714 |
| 1.0 | 1.445 | 0.719 |
| 2.0 | 2.311 | 1.241 |
| 4.0 | 3.239 | 2.207 |
| 6.0 | 3.414 | 2.415 |
| 8.0 | 3.441 | 2.476 |
| 10.0 | 3.501 | 2.503 |
| 12.0 | 3.528 | 2.517 |
| 14.0 | 3.603 | 2.506 |

*Conventional drying shrinkage measurement is conducted at a curing age of 1 day onward, according to ASTM C490-83a. On the other hand, it usually takes only about 2 h for Portland cement to start hardening [44]. In this work, the drying shrinkage was measured at curing ages from 2 h to 14 days.

$$\langle 1-\cos^2\phi\cos^2\theta\rangle = \frac{\pi}{2}\int_{-\frac{\pi}{2}}^{\frac{\pi}{2}}\int_{-\frac{\pi}{2}}^{\frac{\pi}{2}}(1-\cos^3\phi\cos^2\theta)\,d\theta\,d\phi = \pi^2 \tag{17}$$

$$\epsilon_1 = 4\left(\frac{\langle\epsilon_c\rangle}{\pi^2}-\epsilon_2\right) \tag{18b}$$

$$\langle\epsilon_c\rangle = \frac{\pi^2}{4}\epsilon_1 + \pi^2\epsilon_2 \tag{18a}$$

Table 3 gives $\epsilon_c$ and $\epsilon_m$, from which and from Eq. (13) and (18b) $\epsilon_f$ can be calculated. With the above consideration, Eq. (6) and (8) can be rewritten as

$$\tau_e = \frac{E_m}{4(1-2\nu_m)sV_f}K\epsilon_1 \qquad \text{(Slip Model)} \tag{19}$$

$$\tau_{e_{max}} = \frac{1}{2}nE_fK\epsilon_1\tanh(ns) \qquad \text{(No Slip Model)} \tag{20}$$

TABLE 4

Fiber-matrix Interfacial Shear Stress

| Curing age (days) | Stress (MPa) | |
|---|---|---|
| | Slip Model | No Slip Model |
| 0.3 | 0.48 | 1.39 |
| 0.5 | 0.64 | 1.58 |
| 0.75 | 0.75 | 1.75 |
| 1.0 | 0.87 | 1.90 |
| 2.0 | 1.48 | 3.01 |
| 4.0 | 1.64 | 3.11 |
| 6.0 | 1.60 | 3.02 |
| 8.0 | 1.62 | 2.98 |
| 10.0 | 1.69 | 3.10 |
| 12.0 | 1.73 | 3.15 |
| 14.0 | 1.92 | 3.46 |

where

$$n = \left( \frac{2E_m}{E_f(1+\nu_m)\ln(P_f/V_f)} \right)^{1/2}$$

Table 4 shows the calculated results of fiber-matrix interfacial stress at different curing times for the slip model and the no slip model. Fig. 8 are the plots of the data listed in Table 4. From Table 4 and Fig. 8, we can clearly see that, with the increase of the curing time, the drying shrinkage increases and the fiber-matrix interfacial shear stress increases also.

## Discussion

The calculated values of the average shear stress by the slip model is smaller than the maximum shear stress provided by the no slip model, as expected. The slip model is an assumption that makes the mathematical modeling simpler. It is believed that, in the real situation, the carbon fibers will not totally slip under the condition of drying shrinkage. In the design of steel reinforced concrete beams, it is commonly assumed that there is no slip between steel and concrete under load. This assumption largely holds true in practice, though minor slip occurs [45]. For carbon fiber reinforced mortar, no reference was found that mentioned if carbon fiber slipped or not under load or during the shrinkage. Since the carbon fiber surface is much smoother than that a steel bar, and there is little to no bonding with the matrix, it is believed that there should be a certain degree of slippage that occurs during the shrinkage. Therefore, the real situation will involve partial slip.

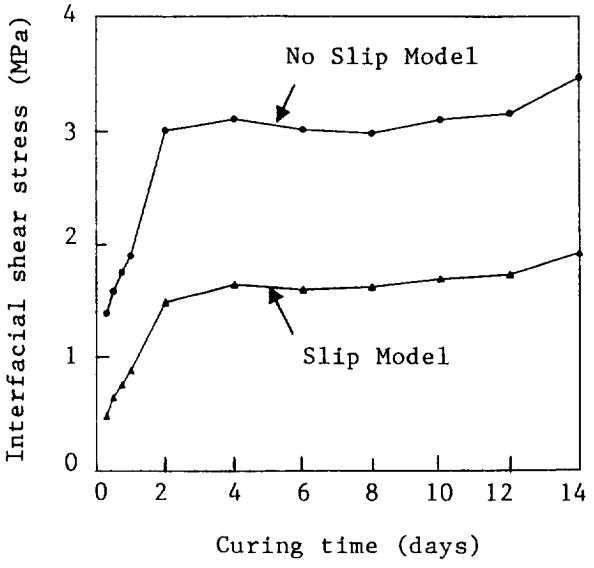


FIG. 8.
Calculated carbon fiber-mortar interfacial shear stress.

The interfacial shear stress discussed here is referred to as the shear stress caused by the drying shrinkage, or the residual stress at the fiber-matrix interface. It is not the pull-out shear strength, which represents the "maximum" interfacial shear strength. Only under the condition of total slipping is the interfacial shear stress equal to the pull-out shear strength. Therefore, the calculated value for using both Slip and No Slip Models should be smaller than the interfacial shear strength. The measured shear strength between carbon fiber and cement is about 6.1 MPa [34]. As compared to the interfacial shear stress calculated by the Slip Model of 1.9 MPa and that by the No Slip Model of 3.5 MPa after 14 days of curing, it is believed the mathematical models derived here have reasonable accuracy.

## References


1. J.I. Daniel and S.P. Shah, Ed., ACI SP-142, Fiber Reinforced Concrete, ACI, Detroit, 1994.
2. D.J. Hannant, Mater. Sci. Tech. 11, 853 (1995).
3. N. Banthia, A. Moncef, K. Chokri and J. Sheng, Can. J. Civ. Eng. 21, 999-1011 (1994).
4. Isabel Padron and Ronald F. Zollo, ACI Mater. J. 87, 327-332 (1990).
5. Pu-Woei Chen and D.D.L. Chung, ACI Mater. J., in press.
6. C.D. Johnson, in Progress in Concrete Technology, edited by V.M. Malhortra, pp. 451-504, Energy, Mines and Resources, Ottawa, Canada, 1980.
7. S. Furukawa, Y. Tsuji and S. Otani, Proc. 30th Japan Congress of Materials Research, Kyoto, Japan, 1987, pp. 149-152.
8. M.A. Swayze, J. Amer. Concr. Inst. 38(4), 425 (1942).
9. S. Giertz-Hedstrom, Proc. 2nd Int. Symp. Chem. Cements, Stockholm, 1938, pp. 505-534.
10. E.K. Rice, G.L. Vondran, and H.D. Kunbargi, Mat. Res. Soc. Symp. Proc. Vol. 114, edited by S. Mindess and S.P. Shah, Materials Research Society, 1988, pp. 145-152.
11. Xuli Fu and D.D.L. Chung, Cem. Concr. Res. 25(7), 1397-1402 (1995).
12. Xuli Fu and D.D.L. Chung, Cem. Concr. Res.26(2), 189-194 (1996).
13. Parviz Soroushian, Fadhel Aouadi and Mohamad Nagi, ACI Mater. J. 88, 11-18 (1991).
14. Amnon Katz, Victor C. Li and A. Kazmer, J. Mater. Civil Eng., May 1995, pp. 125-128.
15. Y. Wang, V.C. Li, and S. Backer, Mat. Res. Soc. Symp. Proc. Vol. 114, 1988, pp. 159-165.
16. A. Kelly and W.R. Tyson, J. Mech. Phys. Solids 13, 329 (1965).
17. H.L. Cox, Br. J. Appl. Phys. 3, 72 (1952).
18. T.F. Cooke, J. Polym. Eng. 7(3), 199 (1987).
19. M.R. Piggott, Load Bearing Fiber Composites, Pergamon Press, New York, 1980.
20. Pu-Woei Chen and D.D.L. Chung, Composites 24, 33-52 (1993).
21. Xiaoming Yang and D.D.L. Chung, Composites 23, 453-460 (1992).
22. Parviz Soroushian, Mohamad Nagi and Jer-Wen Hsu, ACI Mater. J. 89, 267 (1992).
23. H. Nakagawa, S. Akihama, T. Suenaga, Y. Taniguchi and K. Yoda, Adv. Composite Mater. 3, 123 (1993).
24. H.A. Toutanji, T. El-Korchi and R. Nathan Katz, Cem. Concr. Composites 16, 15 (1994).
25. S.B. Park, B.I. Lee and Y.S. Lim, Cem. Concr. Res. 21, 589 (1991).
26. T. Tanaka, K. Yagi, N. Kojima, K. Kimura and H. Katsumata, Adv. Composite Mater. 4, 183 (1994).
27. Sin-Song Lin, SAMPE J. 30, 39 (1994).
28. Pu-Woei Chen and D.D.L. Chung, Composites: Part B 27B, 11-23 (1996).
29. Pu-Woei Chen and D.D.L. Chung, J. Am. Ceram. Soc. 78(3), 816-818 (1995).
30. Pu-Woei Chen and D.D.L. Chung, ACI Mater. J., in press.
31. Pu-Woei Chen and D.D.L. Chung, Smart Mater. Struct. 2, 22-30 (1993).
32. D.D.L. Chung, Smart Mater. Struct. 4, 59-61 (1995).
33. Xuli Fu and D.D.L. Chung, Cem. Concr. Res. 26(1), 15-20 (1996).

34. Xuli Fu and D.D.L. Chung, Cem. Concr. Res. 25(7), 1391-1396 (1995).
35. A. Bentur, Mat. Res. Soc. Symp. Proc. Vol. 114, Materials Research Society, 1988, p. 133.
36. A. Bentur, Proc. Durability of Glass Fiber Reinforced Concrete Symposium, edited by S. Diamond, Prestressed Concrete Institute, Chicago, 1985, pp. 109-123.
37. R.N. Swamy and A.K. Bandyopndhyay, Proc. Inst. C. E., Part 2, Vol. 59, pp. 381-394 (London, Sept. 1975).
38. L.W. Teller, ASTM Spec. Tech. Pub., No. 169, pp. 94-103 (1956).
39. Mingguang Zhu and D.D.L. Chung, Cem. Concr. Res., in press.
40. A.M. Neville, Properties of Concrete, 3rd Edition, Pitman Publishing Inc., MA, 1981.
41. ASTM C-469-75, Test Method for Static Modulus of Elasticity and Poisson's Ratio of Concrete in Compression.
42. A.C. Ugural and S.K. Fenster, in Advanced Strength and Applied Elasticity, Chapter 8, 2nd SI ed., Elsevier, New York, 1987.
43. L.K. Jain and R.C. Wetherhold, Acta. Metall. Mater. 40, 1135 (1992).
44. S. Giertz-Hedstrom. Proc. 2nd Int. Symp. on the Chemistry of Cements, Stockholm, 1938, pp. 504-534.
45. S. Mindess, Mat. Res. Soc. Symp. Proc. Vol. 114, Materials Research Society, 1988, pp. 3-22.